Zhou *et al. Journal of Translational Medicine* (2025) 23:567
https://doi.org/10.1186/s12967-025-06565-5

Journal of Translational Medicine

RESEARCH Open Access

Unveiling the hidden dance: SPP1 + macrophages identified in ulcerative colitis reveal crosstalk with CHI3L1 + fibroblasts

Peiwen Zhou[1], Tongyu Tang[2], Pingwei Zhao[3], Quan Wang[3], Xintong Hu[1], Junzhuo Si[1], Tianshi Yang[1], Shuai Zhou[1], Wenyan An[1] and Yanfang Jiang[1*]

Abstract

Background Ulcerative colitis (UC) is a chronic inflammatory bowel disease characterized by persistent inflammation of the colon. The specific cause of UC is still not fully understood, but this condition is believed to arise from a combination of environmental, genetic, microbial, and immune factors. This study aimed to explore the specific roles of macrophages and fibroblasts in UC pathogenesis, focusing on their interactions and contributions to disease progression.

Methods We utilized single-cell RNA sequencing (scRNA-seq) to analyze macrophages and fibroblasts in peripheral blood and colon biopsy samples from UC patients. Bulk RNA sequencing and spatial transcriptomic data from the Gene Expression Omnibus (GEO) database and flow cytometry and multiplex immunohistochemistry (mIHC) data were used for validation. Statistical analyses were performed to assess the correlation between cell abundance and disease severity.

Results Macrophages and fibroblasts were identified as key communication hubs in UC; specifically, SPP1 + macrophages and CHI3L1 + fibroblasts were significantly enriched at the sites of inflammation. These cells are strongly correlated with disease severity and orchestrate inflammatory responses within the intestinal immune microenvironment, contributing to UC-associated colorectal cancer.

Conclusions Our study identified SPP1 + macrophages and CHI3L1 + fibroblasts as key contributors to UC pathogenesis. These cells are enriched in inflammatory sites, are correlated with disease severity, and play a role in UC-associated colorectal cancer, providing new insights into UC mechanisms.

Keywords Ulcerative colitis, SPP1 + macrophages, CHI3L1 + fibroblasts, Regulatory networks, scRNA-seq

Introduction

Ulcerative colitis (UC) is a type of inflammatory bowel disease (IBD) that is more common than Crohn's disease is [1]. The incidence of UC is increasing annually in Asia, with a fourfold increase in prevalence is expected by 2035 [2]. The most severe complication of UC is colorectal cancer (CRC). Indeed, studies have shown that individuals with UC have a greater risk of developing and dying from CRC than do those without UC [3–5]. Risk factors for UC-associated tumors include a long disease

*Correspondence:
Yanfang Jiang
yanfangjiang@hotmail.com; yanfangjiang@jlu.edu.cn
[1] Genetic Diagnosis Center, The First Hospital of Jilin University, Changchun 130021, China
[2] Department of Gastroenterology, The First Hospital of Jilin University, Changchun 130021, China
[3] Department of Gastrointestinal Surgery, General Surgery Center, The First Hospital of Jilin University, Changchun 130021, China

duration, extensive tumor involvement, and primary sclerosing cholangitis. Therefore, exploring the pathogenesis of UC, controlling the progression of this disease, shortening the course of UC, and reducing the incidence of UC-CRC are important research topics.

The exact pathogenesis mechanism of UC is still under investigation. UC is hypothesized to be caused by a combination of environmental factors, host genetic factors, intestinal microbial infections and immune factors [6, 7]. In other autoimmune diseases, such as psoriasis and rheumatoid arthritis, abnormalities in immune system regulation are strongly correlated with the disease [8]. As the intestinal flora comprises a microbial community, the intestinal immune response to the intestinal flora is strictly regulated and determines the occurrence of immune tolerance or a defensive inflammatory response. Disturbances in the balance of intestinal immune reactions can lead to UC [9, 10].

Single-cell RNA sequencing (scRNA-seq) is used to accurately determine the transcriptional characteristics of individual cells. Multiple studies have described the diverse cell types in the intestinal mucosa of UC patients, highlighting the imbalance in cellular populations in the context of intestinal inflammation [11, 12]. These findings provide valuable insights into the mechanisms underlying UC pathogenesis and will aid in the identification of potential therapeutic targets.

Macrophages are innate immune cells that play important roles in both the inflammatory response and tumor immunity. Various inflammatory cytokines secreted by macrophages play crucial roles in UC [12]. Tumor-associated macrophages, specifically SPP1 + macrophages, have been found in multiple types of cancer. These cells are highly enriched in tumor tissues and are closely associated with prognosis [13–15].

In IBD, disruption of the intestinal mucosal barrier is a key cause of disrupted immune homeostasis. In chronic infections, inflammation, and cancer, the tissue microenvironment regulates the behavior of local immune cells. Among them, fibroblasts in the tissue microenvironment are key cell types that modulate immune responses, either by activating or suppressing them [16]. Intestinal fibroblasts can undergo phenotypic polarization in response to microbial stimuli, shifting toward a proinflammatory state and acting as a central feedback hub to further facilitate immune cell recruitment [17]. In addition, tumor-associated fibroblasts are enriched in CRC and serve as key components of the tumor microenvironment that promote cancer cell invasion and reshape immune cell infiltration pathways [18].

Both macrophages and fibroblasts have been reported as key nodes in intercellular communication within the immune microenvironment of IBD, with each cell type playing a critical role in disease pathogenesis [19–21]. Furthermore, interactions between macrophages and fibroblasts have been well documented in various cancers and inflammatory diseases, where they are closely linked to disease progression [14, 22–24]. However, despite these findings under other conditions, there is limited research on the interactions between macrophages and fibroblasts, especially in UC. Therefore, this study focused on the interactions between macrophages and fibroblasts in UC patients and, for the first time, identified tumor-associated SPP1 + macrophages in UC patients. We observed enrichment of SPP1 + inflammation-associated macrophages and CHI3L1 + inflammation-associated fibroblasts at inflammatory sites in UC patients and found that the infiltration level of these cells is strongly correlated with the severity of the disease in these patients. Immunofluorescence staining confirmed this interaction. Overall, this work reveals interactions between CHI3L1 + fibroblasts and SPP1 + macrophages, which may provide new insights for the diagnosis and treatment of UC.

Methods

Clinical sample collection from patients

Normal mucosal and inflammatory tissue samples as well as fresh peripheral blood samples were collected from UC patients (n = 7). Fresh tissue samples were kept on ice in RPMI 1640 medium supplemented with 10% FBS and prepared for transport. Specific clinical information is provided in Supplementary Table 1.

Primary analysis of the raw read data (scRNA-seq)

The raw reads were processed to generate gene expression profiles via CeleScope v1.12 (Singleron Biotechnologies) with default parameters. Briefly, barcodes and unique molecular identifiers (UMIs) were extracted from R1 reads and corrected. Adapter sequences and poly A tails were trimmed from R2 reads, and the trimmed R2 reads were aligned against the GRCh38 (hg38) transcriptome via STAR (v2.6.1b). Uniquely mapped reads were subsequently assigned to exons with FeatureCounts (v2.0.1). Successfully assigned reads with the same cell barcode, UMI and gene were grouped together to generate a gene expression matrix for further analysis.

Quality control, dimension reduction and clustering (Scanpy)

Scanpy v1.8.2 was used for quality control, dimensionality reduction and clustering in Python 3.7. For each sample dataset, we filtered the expression matrix according to the following criteria: (1) cells with a gene count less than 200 or with a top 2% gene count were excluded; ((2) cells with a top 2% UMI count were excluded; (3) cells

with a mitochondrial content > 30% were excluded; and (4) genes expressed in fewer than 5 cells were excluded. After filtering, 123,092 cells were retained for downstream analyses, with an average of 896 genes and 2362 UMIs per cell. The raw count matrix was normalized by total counts per cell and logarithmically transformed into a normalized data matrix. The top 2000 variable genes were selected by setting flavor = 'seurat'. Principal component analysis (PCA) was performed on the scaled variable gene matrix, and the top 23 principal components were used for clustering and dimensionality reduction. The cells were separated into 23 clusters via the Louvain algorithm, and the resolution parameter was set to 1.2. The cell clusters were visualized via uniform manifold approximation and projection (UMAP)[25].

Batch effect removal

The batch effect between samples was removed with Harmony v1.0 using the top 20 principal components from the PCA [26].

Differentially expressed gene (DEG) analysis (Scanpy)

To identify DEGs, we used the scanpy.tl.rank_genes_groups() function based on the Wilcoxon rank-sum test with default parameters; genes expressed in more than 10% of the cells in either of the compared groups of cells and with an average log(fold change) value greater than 1 were identified as DEGs. The adjusted P value was calculated via Benjamini–Hochberg correction, and a value of 0.05 was used as the criterion to evaluate statistical significance.

Pathway enrichment analysis

To investigate the potential functions of DEGs between inflammatory or ulcerated (IFM) tissue and normal or noninflammatory (non-IFM) tissues, we performed Gene Ontology (GO) and Kyoto Encyclopedia of Genes and Genomes (KEGG) analyses via the "clusterProfiler" R package v 4.0. Pathways with p_adj values less than 0.05 were considered significantly enriched. Data for selected significantly enriched pathways were plotted in bar plots. Gene set enrichment analysis (GSEA) was performed on the DEGs. For gene set variation analysis (GSVA), average gene expression levels for each cell type were used as input data [27]. GO gene sets in the molecular function (MF), biological process (BP), and cellular component (CC) categories were used.

Cell type annotation

Cell type recognition with Cell-ID

Cell-ID is a multivariate approach that extracts gene signatures for each individual cell and performs cell identity recognition using hypergeometric tests (HGTs). Dimensionality reduction was performed on a normalized gene expression matrix through multiple correspondence analysis, in which both cells and genes were projected in the same low-dimensional space. Then, a gene ranking was calculated for each cell to obtain the most featured gene sets of that cell. HGTs were performed on these gene sets against the intestinal reference from the SynEcoSys database, which contains all cell type-specific genes. The identity of each cell was determined as the cell type with the minimal HGT P value. For cluster annotation, the frequency of each cell type was calculated for each cluster, and the cell type with the highest frequency was used to determine cluster identity.

The identity of each cell cluster was determined according to the expression of canonical markers from the reference database SynEcoSysTM (Singleron Biotechnology). SynEcoSysTM contains collections of canonical cell type marker data for single-cell sequencing data from CellMarkerDB, PanglaoDB and recently published literature.

Filtering of cell doublets

The number of cell doublets was estimated on the basis of the expression patterns of canonical cell markers. Any clusters enriched with multiple cell type-specific markers were excluded from the downstream analysis.

Cell–cell interaction (CCI) analysis via CellChat

CellChat (version 1.6.1) was used to analyze intercellular communication networks according to the scRNA-seq data. The CellChat dataset was created using the corresponding R package. Cell information was added to the meta-slot of the object. The ligand–receptor interaction database was used, and matching receptor inference calculations were performed [28].

CCI analysis: CellPhoneDB

CCIs between fibroblasts and macrophages were predicted on the basis of known ligand–receptor pairs via CellPhoneDB (v2.1.7) [29]. The permutation number for calculating the null distribution of average ligand–receptor pair expression in randomized cell identities was set to 1000. Individual ligands or receptor expression levels were thresholded according to a cutoff on the basis of the average log gene expression distribution for all genes across each cell type. Predicted interaction pairs with a P value < 0.05 and an average log expression > 0.1 were considered significant and visualized with a heatmap plot and dot plot, respectively, in CellPhoneDB.

Pseudotime trajectory analysis with Monocle2

The cell differentiation trajectory of monocyte subtypes was reconstructed with Monocle2 v 2.22.0 (ref). For construction of the trajectory, the top 2000 highly variable

genes were selected with the Seurat (v4.1.2) FindVariableFeatures() function, and dimension reduction was performed with DDRTree(). The trajectory was visualized with the plot_cell_trajectory() function in Monocle2 [30].

RNA velocity

For RNA velocity, BAM files containing fibroblasts and macrophages and the reference genome GRCh38 (hg38) were used for analysis with velocyto (v 0.2.4) [31] and scVelo (v0.17.17) in Python with default parameters. The results were projected to the UMAP plot in Seurat clustering analysis for visualization consistency.

UCell gene set scoring

Gene set scoring was performed using the R package UCell v 2.2.0 [32]. UCell scores were determined on the basis of the Mann–Whitney U statistic by ranking query genes in order of their expression levels in individual cells. Because UCell is a rank-based scoring method, it is suitable for use in large datasets containing multiple samples and batches.

scGSVA

To perform GSVA for single-cell data, we used scGSVA (https://github.com/guokai8/scGSVA), which uses ssGSEA methods to score individual cells to generate multiple pathway enrichment score matrices. The limma package was used to calculate the differential enrichment scores for pathways; an absolute value of t greater than 1.96 indicated a significant difference in these scores among cell types.

Transcription factor (TF) regulatory network analysis (pySCENIC)

A TF network was constructed with pySCENIC (v0.11.0) [33] using the scRNA expression matrix and TFs in AnimalTFDB. First, GRNBoost2 was used to construct a regulatory network on the basis of the coexpression of regulators and targets. CisTarget was subsequently used to exclude indirect targets and to search for TF binding motifs. Afterward, AUCell was used for regulon activity quantification for every cell. Cluster-specific TF regulons were identified according to regulon specificity scores (RSSs), and the activity of these TF regulons was visualized in heatmaps.

MuSic

Cell type deconvolution of the bulk RNA-seq data with single-cell references was performed with the R package MuSiC (v1.0.0). The bulk RNA-seq data were deconvoluted to obtain the proportions of cell types in each sample.

Spatial transcriptomic data analysis

Spatial transcriptomic data were obtained from the GEO database (accession number: GSE189184). The data were preprocessed using the Seurat package (v4.0.4) in R. Seurat's FindTransferAnchors and TransferData functions were employed to transfer the scRNA-seq annotation information to the spatial transcriptomic data. Visualization was performed using the SpatialPlot function in Seurat.

Bulk RNA-seq data analysis

Bulk RNA-seq data were obtained from the GEO database (accession number: GSE193677). In R, differential expression analysis was performed to identify the genes most highly expressed by SPP1 + macrophages and CHI3L1 + fibroblasts. Statistical significance was assessed using t tests. Visualization of these top genes was conducted using the ggplot2 package.

For deconvolution of the bulk RNA-seq data, the CIBERSORT package was used to estimate the proportions of individual cell clusters in each sample. Spearman's rank correlation analysis between cell proportions was performed. Differences in cluster proportions among the three groups were evaluated via the Mann–Whitney U test. Visualization of the results was performed with ggplot2 and ComplexHeatmap.

Flow cytometric analysis of human cells

Briefly, fresh human cells from normal mucosa and inflamed tissue were isolated and washed with phosphate-buffered saline (PBS); after centrifugation (336*g*, 5 min, 4 °C), the supernatant was discarded. The cells were stained with fluorophore-conjugated antibodies specific for surface molecules, namely, anti-CD45-BB515 (564,585, BD Biosciences, USA) and anti-CD68-PE (ab303134, Abcam, UK), at room temperature for 30 min in the dark. After the samples were washed twice with PBS, they were fixed and permeabilized with a fixation/permeabilization reagent (BD Cytofix/Cytoperm™, San Diego, CA, USA). After staining with fluorophore-labeled antibodies for intracellular molecules, anti-SPP1-APC (50-9096-42, Thermo Fisher, USA) was used. The samples were examined on a BD Symphony (BD Biosciences). At least 20,000 events per sample were analyzed using FlowJo software (v10.6.2). Statistical analysis was performed with GraphPad Prism 6, and $P < 0.05$ was considered to indicate significance. ns, not significant. *$P < 0.05$, **$P < 0.01$, ***$P < 0.001$, ****$P < 0.0001$.

Multiplex immunohistochemical analysis

Paraffin-embedded tissue slices were obtained from three UC patients and three UC-CRC patients for multiplex

immunohistochemistry (mIHC). Paraffin sections from UC patients were obtained from the patients included in this study for single-cell sequencing, and the detailed clinical data for the UC-CRC patients are shown in Supplementary Table 3. The tissue sections were first deparaffinized by incubation in xylene for 2×10 min, followed by rehydration through graded ethanol (100%, 95%, and 70%) for 5 min each. Antigen retrieval was performed using a microwave at 20% maximum power for 15 min in preheated citrate solution (pH 6.0), and the slides were then cooled to room temperature and washed with Tris-buffered saline (TBS, pH 7.6) for 3×5 min. For mIHC, the following primary antibodies were applied sequentially: anti-SPP1 (Abcam, #ab214050, 1:500), anti-CHI3L1 (Abcam, #ab305035, 1:500), and anti-CD68 (Absinbio, #abc171440, 1:200), each for 30 min at room temperature. After being washed with TBS (3×5 min), the slides were incubated with HRP-conjugated secondary antibodies (anti-rabbit HRP, Absinbio, #A10011-60, 1:200) for 10 min, followed by signal amplification via a TSA 7-color kit (Absinbio, Abs50015-100 T) with TSA570 (1:2000), TSA520 (1:500), and TSA650 (1:200) for the respective markers. Following each round of staining, antigen retrieval was repeated in preheated citrate solution, and the slides were washed again in TBS. After the final round of antibody staining, the slides were incubated with DAPI (Thermo Fisher, D1306, 2 drops) at room temperature for 10 min for nuclear staining, washed in distilled water, air-dried, and mounted with coverslips. Images were captured using the Aperio Versa 8 tissue imaging system (Leica) with a×20 objective lens and analyzed with Indica Halo software (HALO v3.3.2541.424), which quantified the positive staining areas for each marker on the basis of predefined thresholds. For quality control, negative controls were included by omitting the primary antibodies, and isotype controls were used for each round of staining. All experiments were independently repeated with at least three biological replicates to ensure reproducibility.

Results

ScRNA-seq atlas of blood samples and colon biopsies from UC patients

We collected peripheral blood samples and 44 colonoscopy biopsy samples from 7 UC patients (Fig. 1A, Supplementary Table 1). The biopsy tissues from UC patients were divided into normal or noninflammatory (non-IFM) and inflammatory or ulcerated (IFM) tissue groups according to endoscopic assessment. After quality control, 123,092 high-quality single-cell transcribed cells were obtained (quality control information is available in Supplementary Table 2). A total of 44,337 cells from blood samples, 45,533 from IFM samples, and 33,222 from non-IFM samples were sequenced, with a median recovery of 896 genes and 2362 UMIs.

All the cells were visualized via the UMAP technique after batch correction, which revealed epithelial cells, endothelial cells (ECs), fibroblasts, mural cells, proliferating cells, B cells, plasma cells, T cells, neutrophils, mast cells, mononuclear phagocytes (MPs) and erythrocytes (Fig. 1B).

Macrophages in UC

To determine the function of macrophages in UC, we performed secondary clustering of macrophages and identified 5 distinct clusters with clear separation between IFM and non-IFM tissues (Fig. 1C–E). The UMAP dimensionality reduction clustering plot revealed significant intergroup differences in macrophages. The proportions of FCN1 + macrophages and SPP1 + macrophages were increased in the UC IFM tissues, whereas a greater proportion of FHIT + macrophages was found in the UC non-IFM tissues (Fig. 1F, G). Since differences between the IFM and non-IFM groups were observed in several of the five clusters, we initially screened the five macrophage clusters using functional assessment gene set scores (UCell scores) to identify clusters associated with inflammation. We focused on SPP1 + macrophages, which had the highest inflammatory and immune scores among the clusters (Fig. 1H, I).

Next, we studied the gene expression patterns of SPP1 + macrophages. Among the top 10 DEGs (Fig. 1E), the SPP1 gene was uniquely and highly expressed in SPP1 + macrophages. Additionally, IL7R, several MMP family genes (MMP1, MMP10, and MMP12), and certain chemokine ligand genes (CXCL5 and CXCL1) were significantly enriched among SPP1 + macrophages. Assessment of bulk RNA-seq data from the GEO database also revealed high expression levels of the SPP1 gene, MMP genes, and other genes at inflammatory sites (Fig. 1J). Flow cytometry revealed that SPP1 + macrophages were abundant in the inflammatory regions of UC patients (Fig. 1H, Supplementary Fig. 1), and the proportion of SPP1 + macrophages was positively correlated with the levels of clinical markers of inflammation, including circulating CRP, ESR, and IL-6 levels (Fig. 1I). Therefore, we defined the macrophages in this cluster as inflammation-associated SPP1 + macrophages.

SPP1 + macrophages are closely associated with inflammation

As antigen-presenting cells, macrophages play crucial roles in the occurrence, development, and outcome of inflammation via multiple inflammatory pathways [12]. DEGs in macrophages (Fig. 2A) were highly enriched in neutrophil activation and monocyte immune regulation

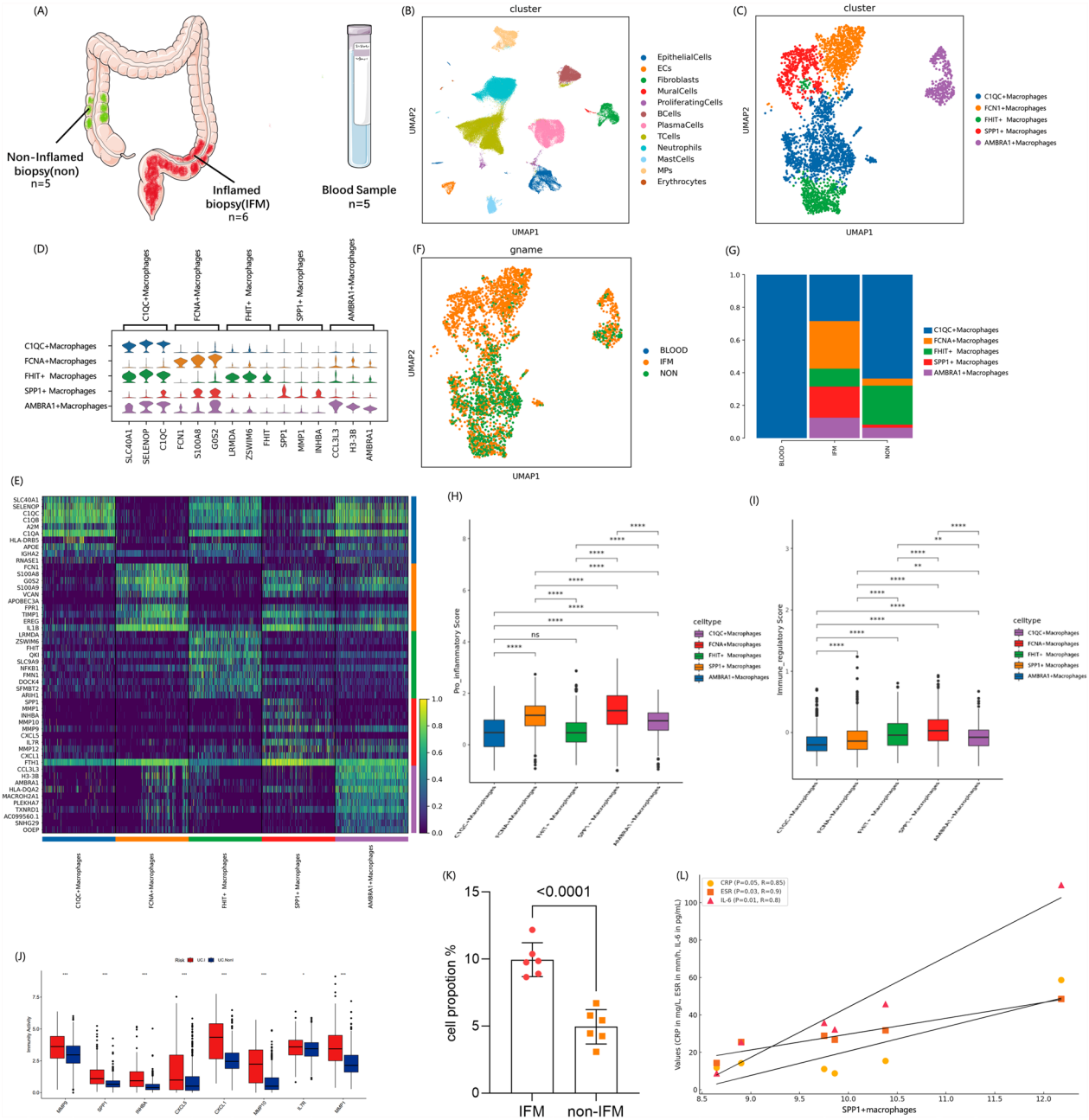

Fig. 1 Single-cell atlas of paired UC blood, IFM tissue and non-IFM tissue samples. **A** Blood, IFM tissue and non-IFM tissue samples from UC patients were processed into single-cell suspensions, and unsorted cells were subjected to scRNA-seq with Singleron Matrix®. **B** UMAP showing 12 clusters in each plot. Each cluster is shown in a different color. **C** UMAP of macrophages colored according to inferred cell type. **D** The top 3 violin vector plots sorted by log fold changes. **E** Heatmap of the top 10 DEGs in different macrophage subsets. **F, G** The distribution (**F**) and proportion (**G**) of each macrophage subset according to different tissue sources. **H, I** UCell scores: Functional assessment gene set scores, such as the proinflammatory score (**H**) and the immunoregulatory score (**I**), were obtained on the basis of the macrophage signature gene set. **J** Bar graphs based on bulk RNA-seq data showing the top 10 DEGs in SPP1 + macrophages at inflammatory (n = 293) and normal tissue sites (n = 579). *P < 0.05, **P < 0.01, ***P < 0.001, and ****P < 0.0001 (P values were calculated by two-sided t tests). **K** Flow cytometric detection of CD68 + SPP1 + macrophages in the rectal inflammatory and noninflammatory tissues of UC patients (n = 6). *P < 0.05, **P < 0.01, ***P < 0.001, and ****P < 0.0001 (P values were calculated by two-sided t tests). **L** Correlation analysis between the CD68 + SPP1 + cell ratio and clinical indicators (n = 6). *P < 0.05, **P < 0.01, ***P < 0.001, and ****P < 0.0001 (P values were calculated by Pearson correlation analysis)

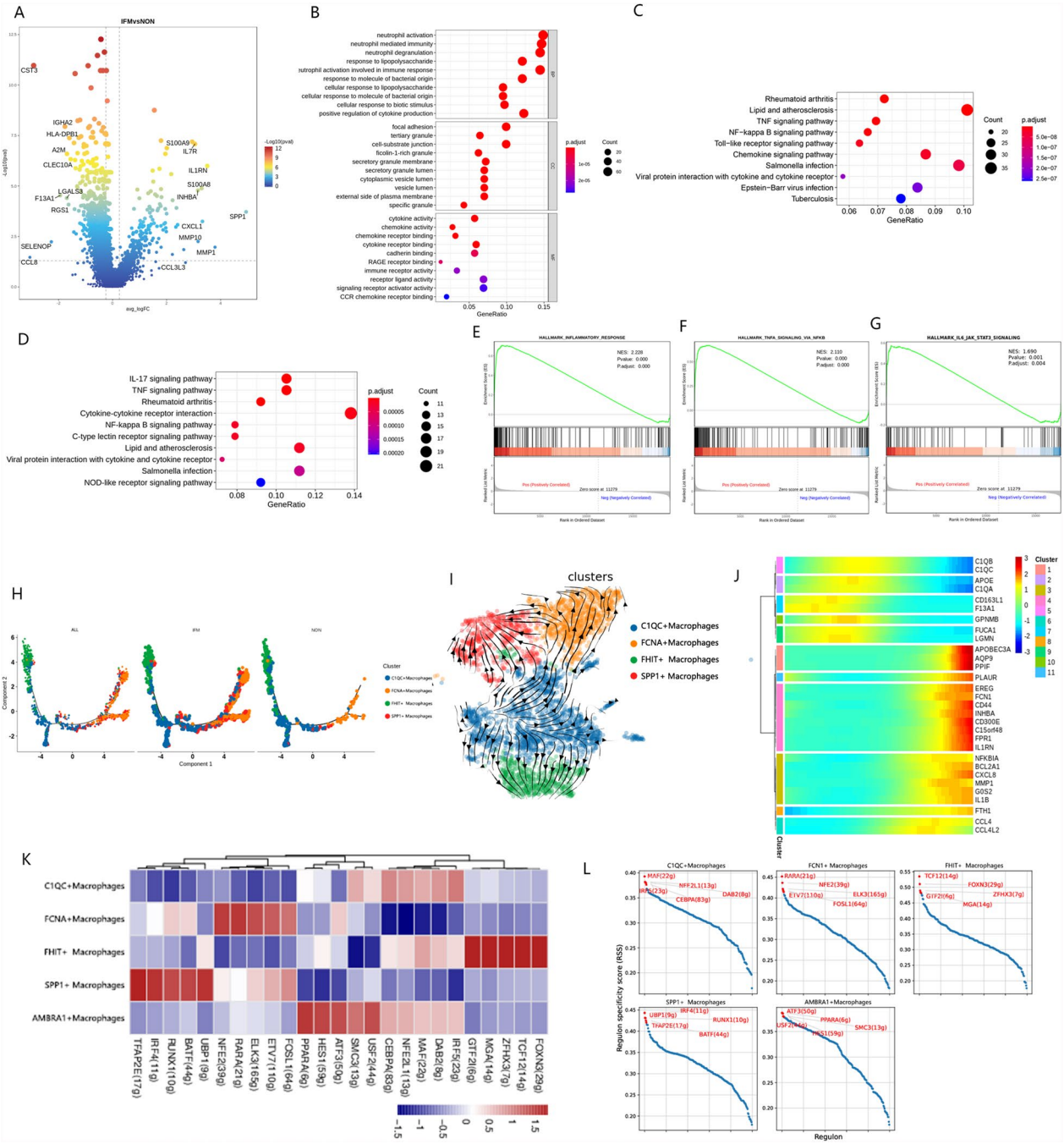

Fig. 2 Characterization of macrophages in non-IFM and IFM tissues. **A** Volcano map showing DEGs in macrophages in non-IFM and IFM tissues. **B, C** GO (**B**) and KEGG (**C**) enrichment analyses of DEGs in macrophages. **D** KEGG enrichment analysis of DEGs in SPP1 + macrophages. **E–G** Pathways significantly enriched according to GSEA. **H** Monocle2 was used to analyze the density distributions of different cell types over time and to fit the pseudotime trajectory between subsets. **I** UMAP plot showing the inferred developmental dynamics of macrophage subsets according to RNA velocity. **J** A situation in which the expression of a gene changes as a function of pseudotime. **K** Heatmap showing the relative expression (z score) of the 5 most highly expressed TFs in each cell subtype. **L** Heatmap of the mean gene expression levels of the top 5 TFs in macrophages

according to GO enrichment analysis, suggesting that macrophages participate in the activation and regulation of cytokines and chemokines (Fig. 2B, Supplementary FIG. 2A). KEGG enrichment analysis revealed strong correlations between DEGs in macrophages and the TNF signaling pathway, the NF–kappa B signaling pathway, the

Toll–like receptor signaling pathway, the chemokine signaling pathway and EB virus infection-related pathways (Fig. 2C, Supplementary Fig. 2B). GO enrichment analysis of the DEGs in SPP1 + macrophages generally revealed enrichment of gene sets generally associated with macrophages, and KEGG enrichment analysis revealed that SPP1 + macrophages were significantly enriched in the IL-17 signaling pathway (Fig. 2D). GSEA also revealed that SPP1 + macrophages were enriched in multiple inflammatory pathways (Fig. 2E–G).

We subsequently conducted RNA velocity and Monocle analyses, which are computational methods based on the newly transcribed RNA in the scRNA-seq datasets, to infer the differentiation trajectory of SPP1 + macrophages. The analysis revealed that SPP + macrophages, almost all of which are present at the site of inflammation, might be derived from C1QC + macrophages and differentiate under the condition of inflammation (Fig. 2H, I, Supplementary Fig. 3A–D), and inflammation-related genes such as NFKB1A, CXCL8, and IL1B were expressed at higher levels at a later time point (Fig. 2J). The differentiation of SPP1 + macrophages is regulated by a complex TF network in which TFs regulate each other and their effector genes through interactions with their cofactors and downstream genes. Therefore, we evaluated the 5 most highly expressed TFs in pySCENIC (Fig. 2K). We found that IRF4 was highly expressed and had the highest regulatory level in the regulatory network of SPP1 + macrophages (Fig. 2L). IRF4 is an effective regulatory factor that was first discovered to regulate interferon transcription and is involved in the differentiation and development of immune cells.

Fibroblasts in UC

We next focused on fibroblasts. A total of 5986 fibroblasts were clustered and divided into eight heterogeneous subgroups via unsupervised dimensionality reduction (Fig. 3A–C). On the basis of the UMAP clustering plot, fibroblasts were found to exhibit intergroup differences, with CHI3L1 + fibroblasts being highly enriched in the UC IFM tissues (Fig. 3D, E). As in a previous study, we first evaluated inflammation-related subgroups using functional enrichment gene set scoring. As expected, according to the UCell scores of the characteristic fibroblast genes, the inflammation score and extracellular matrix (ECM) remodeling score for the CHI3L1 + fibroblasts were the highest (Fig. 3F, G). Therefore, we next focused on CHI3L1 + fibroblasts.

We analyzed the gene signatures of the CHI3L1 + fibroblasts identified in this study. According to the heatmap of the top 10 DEGs (Fig. 3C), CHI3L1 + fibroblasts presented high expression levels of CHI3L1, MMP family genes (MMP3, MMP1, and MMP10), and chemokine ligand genes (CXCL1, CXCL8, CXCL3, and CXCL2). This gene expression pattern was highly consistent with that of SPP1 + macrophages. CHI3L1 is involved in the development of inflammation and plays an important role in the pathogenesis of CD4 + T-cell polarization and Th2 inflammation [34]. Furthermore, differential gene expression analysis between the groups revealed significant differences in the expression of CHI3L1, MMP10, and various chemokine ligand genes between inflammatory and noninflammatory sites (Fig. 3H). We also observed this phenomenon in the bulk RNA-seq dataset, which revealed high expression levels of CHI3L1, MMP, and other genes at inflammatory sites in UC patients (Fig. 3I). Increased expression and activity of MMPs lead to abnormal ECM remodeling, and high expression of inflammatory chemokines triggers abnormal inflammatory regulation [35]. Therefore, we defined CHI3L1 + fibroblasts as inflammation-associated CHI3L1 + fibroblasts.

CHI3L1 + fibroblasts in the inflammatory region in UC patients exhibit a high inflammatory state

First, we performed functional enrichment analysis of the DEGs between the IFM and non-IFM groups in all fibroblast clusters. We found that these genes were highly enriched in the IL-17 signaling pathway, the TNF signaling pathway, cytokine activity, and chemokine activity (Fig. 4A, Supplementary Fig. 4A). After focusing on the CHI3L1 + fibroblasts, GO and KEGG analyses revealed that the DEGs were also enriched in the IL-17 signaling pathway, cytokine activity, and chemokine activity, which was highly consistent with the functional enrichment results for SPP1 + macrophages. In addition, CHI3L1 + fibroblasts are associated with endoplasmic reticulum stress, the ERAD pathway, and neutrophil aggregation (Fig. 4B, C; Supplementary Fig. 4B, C). GSEA revealed that CHI3L1 + fibroblasts correlated with the inflammatory immune response, IFN-γ response, and TNF-NFKB gene sets (Fig. 4D–G). These findings collectively suggest that CHI3L1 + fibroblasts play a proinflammatory role in inflammatory areas in UC patients. Pseudotime analysis indicated that CHI3L1 + fibroblasts are associated with the terminal differentiation stage of UC (Fig. 4H–J, Supplementary Fig. 5A, B). PySCENIC analysis of fibroblasts revealed a strong correlation with the TF MYC (Fig. 4N, O). GSVA revealed that MYC_TARGETS_V1 and MYC_TARGETS_V2 were enriched in CHI3L1 + fibroblasts (Fig. 4P). MYC has been reported to regulate the polarization of inflammatory macrophages and participate in the inflammatory response [36].

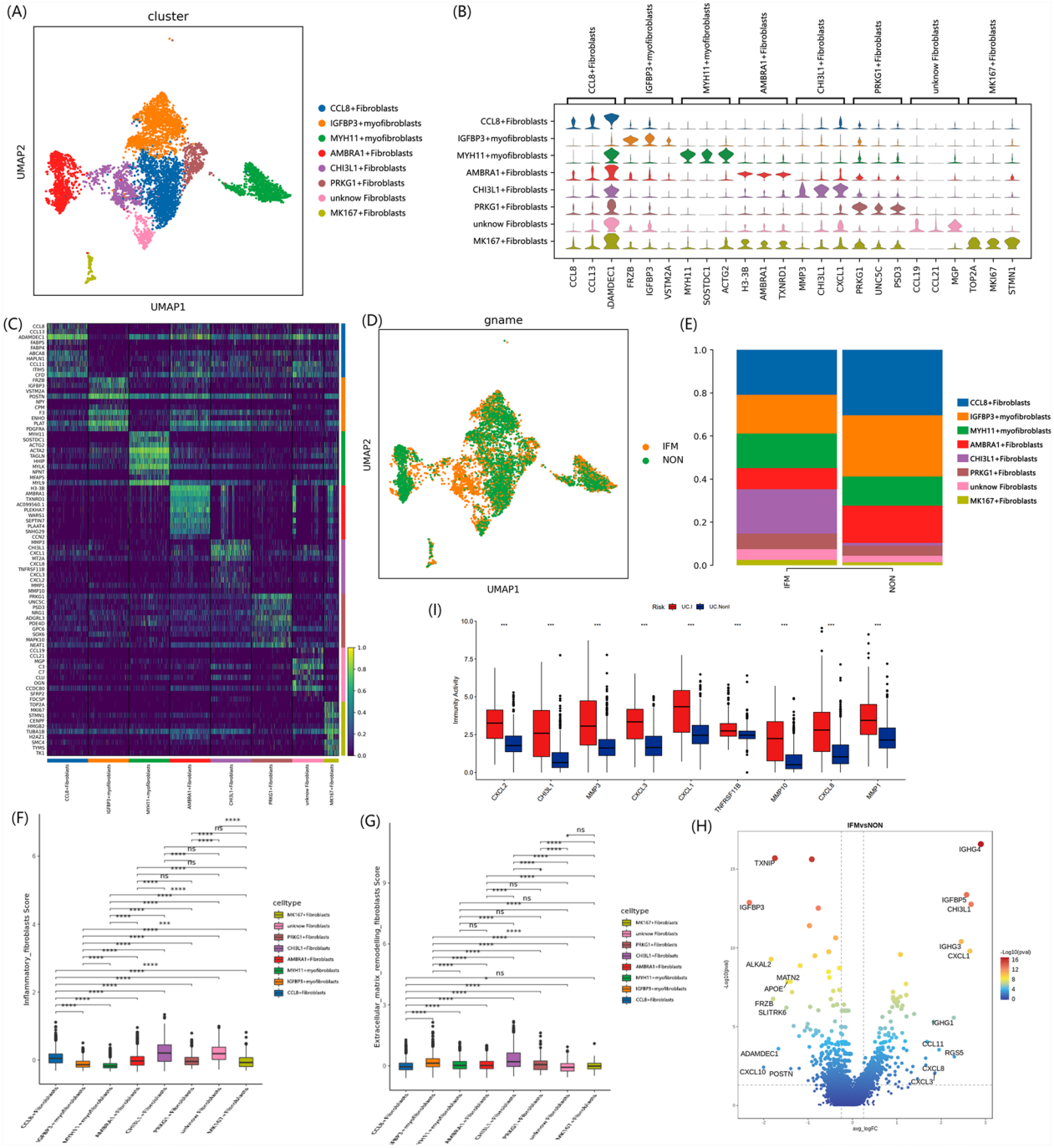

Fig. 3 Dissection of fibroblasts showing the expansion of CHI3L1 + fibroblasts at inflammatory sites. **A** UMAP of fibroblasts colored according to inferred cell type. **B** The top 3 violin vector plots sorted by log fold changes were used to distinguish fibroblast types. **C** Heatmap of the top 10 DEGs in different fibroblast subsets. **D, E** The distribution (**D**) and proportion (**E**) of each fibroblast subset in different tissues. **F, G** UCell scores: Functional assessment gene set scores, such as the proinflammatory score (**F**) and ECM remodeling score (**G**), were obtained on the basis of the fibroblast signature gene set. **H** Volcano map showing DEGs in fibroblasts between non-IFM and IFM tissues. **I** Bar graphs based on bulk RNA-seq data showing the differential expression of the top 9 genes in CHI3L1 + fibroblasts at inflammatory (n = 293) and normal tissue sites (n = 579). *P < 0.05, **P < 0.01, ***P < 0.001, and ****P < 0.0001 (P values were calculated via two-sided t tests)

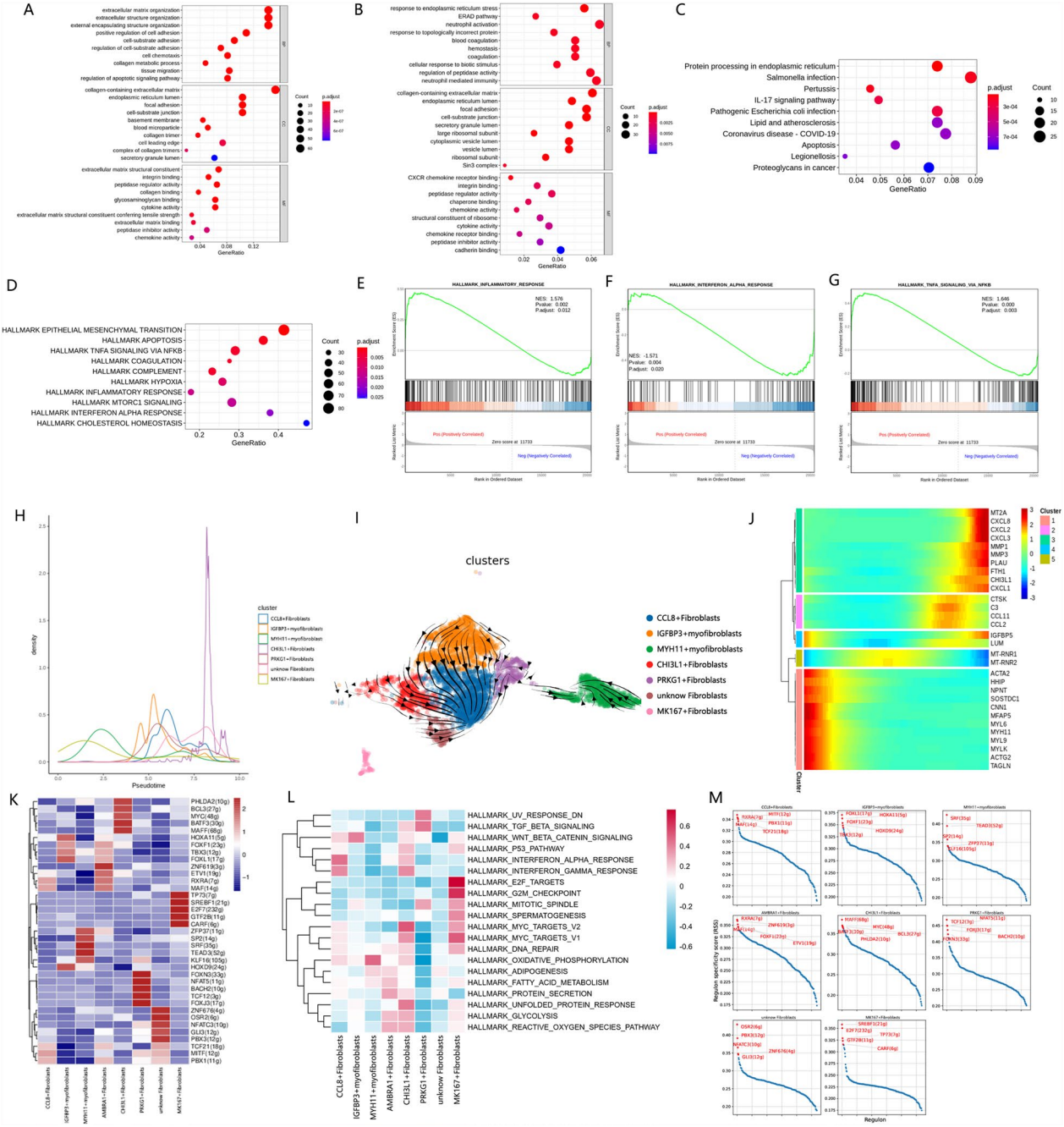

Fig. 4 Characterization of fibroblasts in non-IFM and IFM tissues. **A** GO enrichment analysis of DEGs in fibroblasts. **B, C** GO (**B**) and KEGG (**C**) enrichment analyses of DEGs in CHI3L1 + fibroblasts. **D–G** Pathways significantly enriched according to GSEA. **H** Monocle2 was used to analyze the density distributions of different cell types over time. **I** UMAP plot showing the inferred development dynamics of fibroblast subsets according to RNA velocity. **J** A situation in which the expression of a gene changes as a function of pseudotime. **K, L** Heatmap showing the relative expression (z score) of the top 5 highly expressed TFs (**K**) and related pathways (**L**) in each cell subtype. **M** Heatmap of the mean expression levels of the top 5 TF genes in fibroblasts

Interaction between fibroblasts and macrophages in UC

On the basis of the high consistency and mutual interaction of SPP1 + macrophages and CHI3L1 + fibroblasts in terms of gene enrichment and signaling pathway enrichment, we speculated that there is a mutual interaction between fibroblasts and macrophages in the inflammatory areas of UC and that SPP1 + macrophages and CHI3L1 + fibroblasts play a central role. First, we used

CellPhoneDB to calculate the average expression level of ligands between the two cell populations as an indicator of interaction. Overall, there was a strong ligand–receptor interaction between the MPs and fibroblasts (Fig. 5A). Upon further subdivision into secondary subgroups, the CHI3L1 + fibroblasts clearly exhibited stronger interactions with macrophages than did the other fibroblast subgroups (Fig. 5B). Further meticulous examination of the interaction between ligands and receptors revealed a significant association between CHI3L1 + fibroblasts serving as ligands and FGF2_CD44 ligand–receptor pairs (Fig. 5C), thus highlighting the robust interplay between CHI3L1 + fibroblasts and SPP1 + macrophages. Research has underscored the role of fibroblast growth factor 2 (FGF2) in engaging with CD44 to facilitate the transformation of macrophages into tumor-associated macrophages [37]. Additionally, CHI3L1 + fibroblasts engage extensively with macrophages through the CSF3_CSF3R and CSF3_CSF1R pathways (Fig. 5C). When CHI3L1 + fibroblasts assume the role of receptors, robust cellular communication is observed between SPP1 + macrophages and CHI3L1 + fibroblasts, particularly on the SPP1_CD44 ligand pair. Furthermore, the SPP1_PTGER4 and TNF_DAG1 ligand–receptor pairs exhibited marked interactions (Fig. 5D). Notably, this intricate cellular communication is absent in non-IFM tissues (Fig. 5E, F). To further demonstrate the interactive relationship between fibroblasts and macrophages, we created a network graph of intercellular interactions using CellChat, highlighting the central positioning of CHI3L1 + fibroblasts and SPP1 + macrophages within the network (Fig. 5G).

To assess the spatial distribution of CHI3L1 + fibroblasts and SPP1 + macrophages, we utilized spatial transcriptomic data from patients with active UC obtained via the 10X Visium platform under the GEO accession number GSE189184. The annotation information derived from scRNA-seq was mapped onto two spatial transcriptomic tissue sections. In the resulting spatial maps, CHI3L1 + fibroblasts and SPP1 + macrophages were observed in active UC, with CHI3L1 + fibroblasts encircling SPP1 + macrophages. Both cell types were distributed throughout the lamina propria of the intestinal mucosa (Fig. 5H). Using mIHC technology, we found that CD68 + SPP1 + cells and CHI3L1 + cells at inflammatory sites in UC patients are highly proximal, indicating potential crosstalk between these cell types (Fig. 5I and Supplementary Fig. 6). Furthermore, we screened patients with a long history of UC accompanied by CRC (Supplementary Table 3) and conducted mIHC staining. The results also demonstrated that CD68 + SPP1 + cells and CHI3L1 + cells were spatially close in UC-CRC patients (Fig. 5J and Supplementary Fig. 7).

The presence of SPP1 + macrophages and CHI3L1 + fibroblasts can be used as indicators of clinical severity

Next, we used the GEO dataset GSE193677 to categorize UC patients into nonactive, stable, moderate, and severe UC groups and analyzed the relationships between SPP1 + macrophages and CHI3L1 + fibroblasts and UC severity. The expression levels of almost all of the top 10 genes increased as disease severity increased (Fig. 6A–D). By using deconvolution analysis, we calculated the ratio of SPP1 + macrophages to CHI3L1 + fibroblasts, and, unsurprisingly, both were positively correlated with disease severity (Fig. 6E, F). We further divided UC patients into a treatment response group and a nonresponse group using infliximab and ustekinumab. The results revealed a significant increase in the expression of the top genes in SPP1 + macrophages and CHI3L1 + fibroblasts in the treatment response group (Fig. 6G–J). These findings suggest that SPP1 + macrophages and CHI3L1 + fibroblasts influence the response to immunotherapy, with higher levels of SPP1 + macrophages and CHI3L1 + fibroblasts indicating a better response to immunotherapy.

Discussion

UC is a chronic IBD characterized by persistent inflammation of the intestinal tract and aberrant immune responses. Although the exact etiology of UC remains unclear, an exaggerated immune reaction has been shown to play a pivotal role in the pathogenesis and progression of this disease [2]. The underlying mechanisms of UC are complex and involve intricate interactions among various immune cells and cytokines [38, 39]. While current therapeutic strategies can control symptoms in some patients, more than half of patients still experience chronic, continuous, or relapsing disease, with variable treatment responses due to individual differences [40, 41]. Therefore, a deeper understanding of the immune microenvironment and pathological mechanisms of UC, particularly intercellular interactions, is essential for identifying the root causes of this disease and developing more precise therapeutic approaches. Single-cell transcriptomics offers an unprecedented opportunity to comprehensively analyze the immune microenvironment of UC patients at single-cell resolution and reveals novel directions for future research and therapeutic intervention. Through integrated analyses of scRNA-seq data, publicly accessible bulk RNA-seq and spatial transcriptomic datasets, and mIHC data from patients treated with biologic agents, our study revealed the comprehensive landscape of the microenvironment of inflammatory tissue and adjacent normal tissue at single-cell resolution.

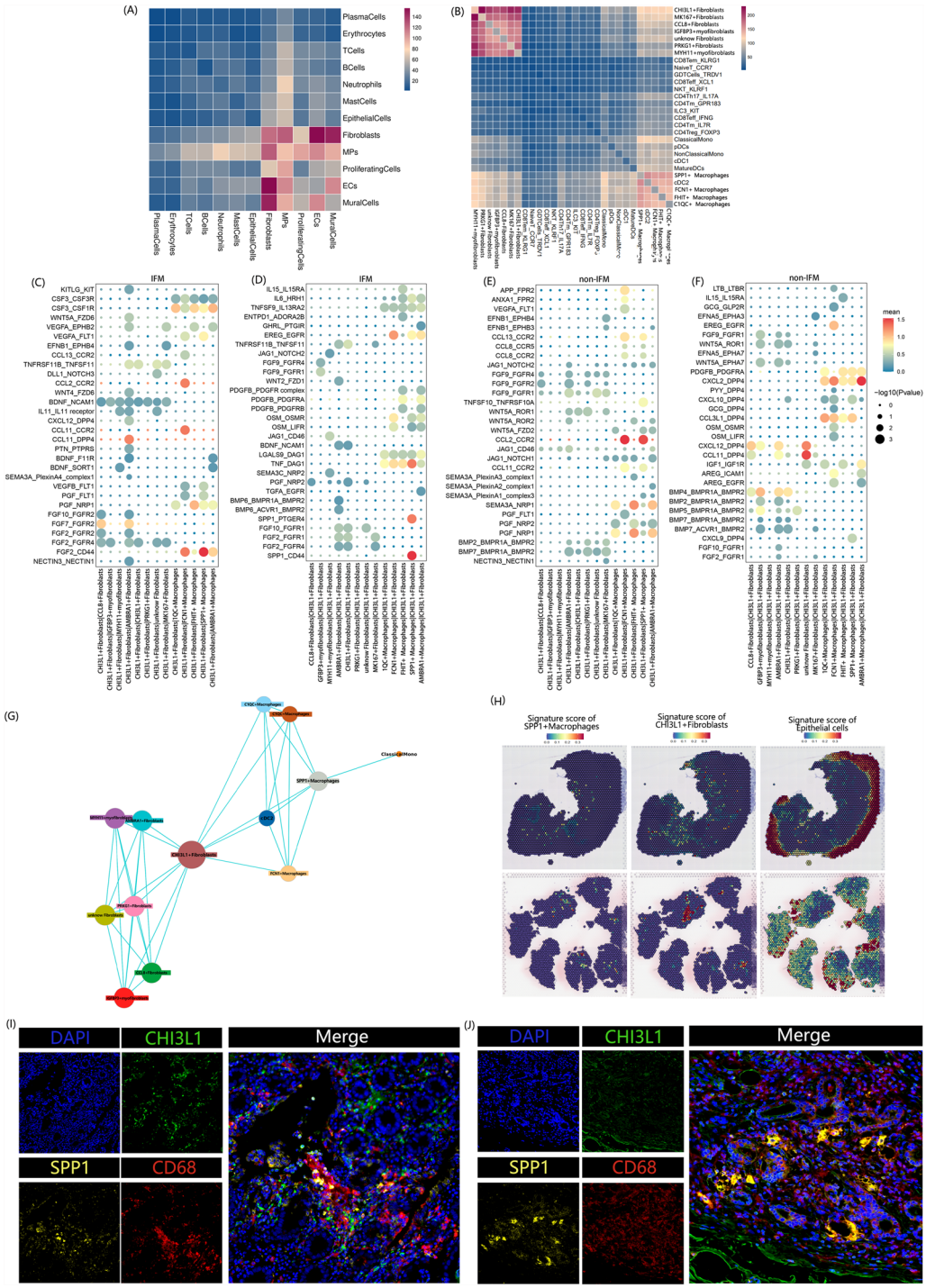

Fig. 5 Interaction network between CHI3L1 + fibroblasts and SPP1 + macrophages. **A, B** Heatmap showing the number of pairwise receptor–ligand interaction pairs for each cell type according to CellPhoneDB. **C**, **D** Receptor–ligand interaction pair bubble plot for the IFM group presenting the top 30 receptor–ligand pairs screened on the basis of the cell type pairs on the abscissa of this plot. **E**, **F** Receptor-ligand interaction pair bubble plot for the non-IFM group presenting the top 30 receptor-ligand pairs screened on the basis of the cell type pairs on the coordinates of this plot. **G** Diagram of the interaction network between cells generated by CellPhoneDB using the top 6 genes; cutoff = 0.1. **H** Spatial feature plots of the signature scores of CHI3L1 + fibroblasts, SPP1 + macrophages and epithelial cells in tissue sections. **I, J** Representative IF images of human UC (**I**) and UC-CRC (J**)** tissues (20x). DAPI (blue), CHI3L1 (green), SPP1 (yellow), and CD68 (red) are shown in individual and merged channels

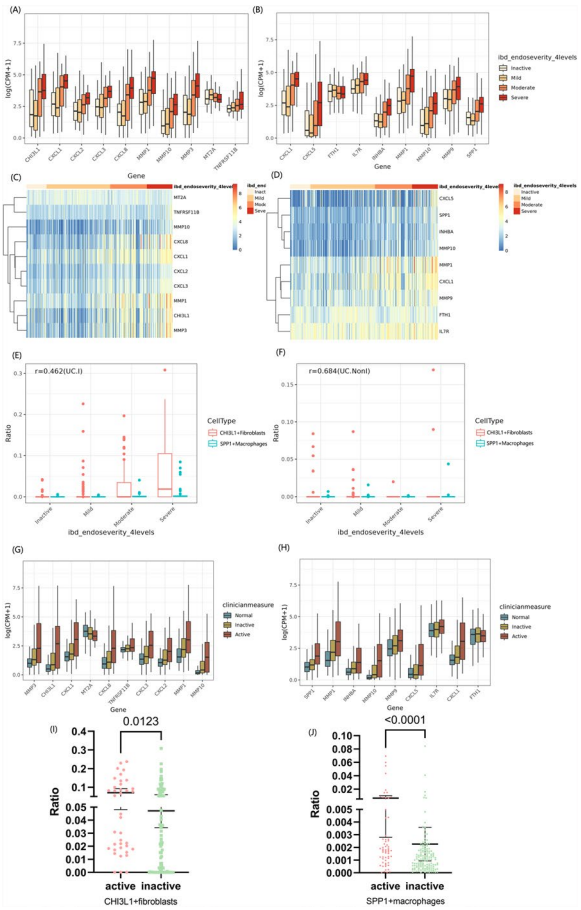

Fig. 6 CHI3L1 + fibroblast and SPP1 + macrophage infiltration according to disease severity and biological treatment response. **A–D** Bar graphs and heatmaps based on bulk RNA-seq data showing differential expression of the genes most highly expressed in CHI3L1 + fibroblasts (**A**, **C**) and SPP1 + macrophages (**B**, **D**) at the 4 disease severity levels. **E**, **F** Histograms of SPP1 + macrophage and CHI3L1 + fibroblast proportions and correlations between groups according to different severities of inflammatory (**E**) and noninflammatory tissue (**F**) after deconvolution on the basis of bulk RNA-seq data (R values were calculated via Spearman correlation). **G, H** Bar graphs based on bulk RNA-seq data showing the differential expression of the top genes in CHI3L1 + fibroblasts (**G**) and SPP1 + macrophages (**H**) in the active and inactive groups according to their response to biologics. **I** Scatter plot diagrams of the ratios of CHI3L1 + fibroblasts in the active (n = 38) and inactive (n = 87) groups according to the response to biologics. **J** Scatter plot diagrams of the ratios of SPP1 + macrophages in the active (n = 60) and inactive (n = 140) groups according to the response to biologics. *P < 0.05, **P < 0.01, ***P < 0.001, and ****P < 0.0001 (P values were calculated by the Mann–Whitney test)

Notably, we reported, for the first time, inflammation-associated SPP1 + macrophages in UC and proposed that there is crosstalk between SPP1 + macrophages and surrounding CHI3L1 + fibroblasts, which affects the disease process.

Through scRNA-seq analysis, an enriched population of SPP1 + macrophages was identified for the first time in the inflammatory regions of UC patients, and these cells were defined as inflammation-associated SPP1 + macrophages. These SPP1 + macrophages exhibit high expression levels of the IL-7R gene, MMP family genes, and several chemokine genes. MMPs are capable of degrading various protein components of the ECM, thereby disrupting the intestinal tissue barrier [42]. Previous studies have shown that the levels of MMP-2, MMP-9, and inflammatory factors are significantly elevated in active UC patients, leading to increased intestinal mucosal permeability and further promoting the progression of UC [43]. Furthermore, SPP1 + macrophages are functionally enriched for inflammatory responses. Although previous single-cell transcriptomic studies on SPP1 + macrophages have been conducted [14, 44, 45], most of these studies focused on the tumor microenvironment, where SPP1 + macrophages promote the proliferation of prostate intraepithelial neoplasia (PIN) cells and the development of prostate cancer through the activation of the Akt and JNK pathways [39]. The infiltration of SPP1 + macrophages has been widely recognized as a key prognostic factor in various cancers [11, 12]. Additionally, the activation of $SPP1^{hi}$ macrophages has been observed in patients with idiopathic pulmonary fibrosis, where it plays a crucial role in the progression of pulmonary fibrosis [45]. The proportion of infiltrating SPP1 + macrophages was positively correlated with the severity of UC, as validated by flow cytometry. Given the increased incidence of CRC in UC patients, we hypothesized that this macrophage subset may play an important role in both the progression of UC and its carcinogenesis.

The heterogeneity of fibroblasts plays an important role in regulating the immune microenvironment, and different stromal cell groups may play different roles in the development of IBD. For example, an activated fibroblast population was reported to have proinflammatory characteristics, exacerbating inflammation and barrier dysfunction [46]. Martin et al. identified a distinct subset of activated fibroblasts in Crohn's disease lesions; these cells were characterized by NCR2 ligand expression (CCL2/CCL7) and functional interactions with monocyte subsets expressing S100A8/S100A9/S100A4 [47]. Inflammatory fibroblasts expressing IL13RA2 and IL11 are associated with resistance to TNF therapy in IBD patients [19]. In Crohn's disease, CXCL14 + and MMP/WNT5A + fibroblasts have been reported to display central signaling in CD strictures and to contribute to a poor prognosis [21]. Intestinal fibroblasts can reshape the cytokine milieu through IL-1β-TLR-NFκB axis activation and remodel the extracellular matrix (ECM) via MMP13-mediated collagen degradation, ultimately establishing

a self-sustaining cycle of chronic inflammation [16]. We found a highly enriched subtype of CHI3L1 + fibroblasts in the inflammatory tissue of UC patients, which also exhibited enrichment of inflammation-associated functions. CHI3L1 is strongly induced during late-stage macrophage differentiation in humans, during which nuclear Sp1 binds to the CHI3L1 promoter, promoting late-stage maturation of human macrophages [48]. Moreover, CHI3L1 can mediate tumor-associated inflammation by activating the MAPK signaling pathway to increase IL-8 and CCL2 expression in SW480 cells and by phosphorylating IL-8, MMP-2, MMP-9, CCL2, CXCL2, and other proinflammatory mediators at the tumor site [34, 49, 50]. In our study, profiling of CHI3L1 + fibroblasts revealed upregulated expression of multiple proinflammatory mediator genes and enrichment of several signaling pathways directly related to the MAPK pathway, such as the TNF signaling pathway, which is consistent with the findings concerning CHI3L1 in tumors described above.

Macrophages and fibroblasts play important roles as components of the intestinal immune microenvironment. When the immune balance is disrupted, interactions between these two cell types collectively promote inflammation. A previous study reported that FAP + fibroblasts may promote the differentiation of THBS1 + macrophages into SPP1 + macrophages through the RARRES2/CMKLR1 interaction, leading to connective tissue proliferation [14].

This study revealed an interaction between SPP1 + macrophages and surrounding CHI3L1 + fibroblasts at inflammatory sites in UC patients that triggers an intestinal inflammatory response. According to our analysis, SPP1 + macrophages and CHI3L1 + fibroblasts exhibit a high degree of overlap in the enrichment of proinflammatory mediators and inflammation-related signaling pathways. In previously reported spatial transcriptomic studies of UC, the authors described a high degree of spatial correlation between CD68 + CHI3L1 + inflammatory fibroblasts and inflammation-associated macrophages [20]. Our analysis revealed that CHI3L1 + fibroblasts spatially surround SPP1 + macrophages, with both cell types scattered throughout the lamina propria of the intestinal mucosa in active UC. In addition, our mIHC results revealed spatial proximity between CHI3L1 + fibroblasts and SPP1 + macrophages at the ulcer site in colorectal tissues from UC patients.

To explore the mechanism of interaction between macrophages and fibroblasts, we performed cell communication analysis via CellPhoneDB. On the basis of this analysis, we hypothesize that the interaction between SPP1 + macrophages and CHI3L1 + fibroblasts in UC may be influenced by the complex relationships among FGF2, CD44, and SPP1. Previous mouse model studies have shown that a lack of FGF2 exacerbates colitis, highlighting its role in macrophage programming and as an immune regulator in the tumor microenvironment [37]. Additionally, FGF2 has been found to promote gastric cancer progression by driving tumor-associated macrophage infiltration [51]. In bladder cancer, inflammatory cancer-associated fibroblasts (CAFs) secrete FGF2, which acts on the CD44 receptor of tumor stem cells, sustaining tumor stemness and epithelial–mesenchymal transformation [52]. The SPP1–CD44 interaction has been well documented in various cancers, such as gastric cancer, where it accelerates malignant progression through crosstalk between SPP1 + macrophages and cancer cells [53]. Similarly, in liver cancer, SPP1 mediates crosstalk between hepatocellular carcinoma cells and macrophages via SPP1-CD44 [54]. Moreover, CD44 and FGF2 receptors, such as FGFR2, regulate gastric cancer cell growth through the c-myc protein regulatory circuit [55].

Following CellPhoneDB analysis, which revealed potential interactions between SPP1 + macrophages and CHI3L1 + fibroblasts, we further explored the relationships between these cell types and TFs using PySCENIC analysis. PySCENIC analysis revealed a strong correlation between CHI3L1 + fibroblasts and the TF MYC and a strong correlation between SPP1 + macrophages and IRF4. Seyeon et al. reported that the MYC/LDH/IRF4 axis plays a role in the polarization of inflammatory macrophages, indicating a link between metabolic reprogramming and the function of inflammatory macrophages [36]. In addition, the MYC/IRF1 axis has been shown to be involved in immune escape and tumor progression in patients with CRC or hepatocellular carcinoma [56, 57]. Based on our findings of several tumor-associated pathways and TFs in UC, we further performed mIHC on intestinal tissue sections from CRC patients with a history of UC and determined the spatial proximity between CHI3L1 + fibroblasts and SPP1 + macrophages. These findings suggest that the two cell subtypes identified in this study—SPP1 + macrophages and CHI3L1 + fibroblasts—may play important roles in the concurrent development of UC and CRC.

Finally, we analyzed the associations between the clinical outcomes and clinical characteristics of patients grouped according to the proportions of CHI3L1 + fibroblasts and SPP1 + macrophages. Data from the GEO database confirmed that the ratio of CHI3L1 + fibroblasts to SPP1 + macrophages was positively correlated with the severity of UC. A greater proportion of SPP1 + macrophages and CHI3L1 + fibroblasts is associated with a better immunotherapy response, particularly in cohorts treated with infliximab and ustekinumab. These findings suggest that the levels of SPP1 + macrophages and CHI3L1 + fibroblasts may serve as potential indicators for

predicting the response to immunotherapy. Infliximab and ustekinumab alleviate inflammatory responses by inhibiting the activity of proinflammatory cytokines such as TNF-α, IL-12, and IL-23 [58, 59]. On the basis of these findings, we hypothesize that in patients with a greater proportion of SPP1 + macrophages and CHI3L1 + fibroblasts, immunotherapy may be more effective in correcting the immune dysregulation induced by these cells, thereby increasing the efficacy of immunotherapy.

This study has several limitations. First, unfortunately, we did not collect samples from UC-CRC patients for scRNA-seq. We plan to further expand the UC-CRC patient cohort and clarify the single-cell transcriptional landscape of UC-CRC patients in subsequent studies. Second, we did not find enough transcriptomic data from UC-CRC patients in the public database. A detailed description of CHI3L1 + fibroblasts and SPP1 + macrophages in UC-CRC patients in this study will be provided in future studies. Moreover, we were unable to obtain patient samples after immunotherapy for additional analysis. In future work, we plan to collect post-immunotherapy samples to investigate the role of SPP1 + macrophages and CHI3L1 + fibroblasts in the mechanisms underlying the immunotherapy response.

Abbreviations

UC	Ulcerative colitis
IBD	Inflammatory bowel disease
CRC	Colorectal cancer
GSEA	Gene set enrichment analysis
TF	Transcription factor
ECM	Extracellular matrix
DEGs	Differentially expressed genes
GSVA	Gene set variation analysis
mIHC	Multiplex immunohistochemistry
scRNA-seq	Single-cell RNA sequencing
PIN	Prostate intraepithelial neoplasia
TME	Tumor microenvironment
UMAP	Uniform manifold approximation and projection
GO	Gene Ontology
KEGG	Kyoto Encyclopedia of Genes and Genomes
MF	Molecular function
BP	Biological process
CC	Cellular component

Supplementary Information

The online version contains supplementary material available at https://doi.org/10.1186/s12967-025-06565-5.

Supplementary materials 1.

Supplementary materials 2.

Acknowledgements

We sincerely appreciate the financial support that made this research possible. I would like to express my gratitude to Li Ang for providing valuable ideas and insights that substantially contributed to the direction of this research. I also extend my thanks to He Jiaxue for assisting with the documentation work, which was crucial in ensuring the smooth progress of the project. Additionally, I am grateful to Chen Liguo for offering essential guidance on data storage, which helped in managing and organizing the research data effectively.

Author contributions

Peiwen Zhou: Writing–review & editing, writing–original draft, visualization. Tongyu Tang: Writing–review & editing, supervision, investigation, resources. Pinwei Zhao: Writing–review & editing, supervision, investigation, resources. Quan Wang: Writing–review & editing, supervision, investigation, resources. Xintong Hu: Writing–original draft, data curation, conceptualization. Junzhuo Si: Writing–original draft, software, methodology, formal analysis. Tianshi Yang: Writing—original draft, methodology, investigation. Shuai Zhou: Writing—original draft, investigation, formal analysis. Wenyan An: Writing–original draft, validation, methodology. Yanfang Jiang: Writing–review & editing, validation, supervision, project administration.

Funding

This research was funded by the National Natural Science Foundation of China (nos. 22174137), the Jilin Province Science and Technology Agency (nos. 2023C013, JJKH20211210KJ, JJKH20211164KJ, JLSWSRCZX2020-009, 20200901025SF and 20200403084SF), and the Beijing Medical Award Foundation (YXJL-2021–1097-0645).

Data availability

The raw single-cell RNA-seq and spatial transcriptomic data generated in this study were deposited in the Genome Sequence Archive with accession ID HRA006540. Since these data are related to human genetic resources, the raw data can be obtained by request and used following the guidelines for the Genome Sequence Archive for noncommercial use at https://ngdc.cncb.ac.cn/gsa-human/request/HRA006540. There are no time restrictions once access has been granted. The guidance for making a data access request for the GSA for humans can be downloaded from https://ngdc.cncb.ac.cn/gsa-human/document/GSA-Human_Request_Guide_for_Users_us.pdf. The processed public RNA-seq dataset was downloaded from GEO (accession number GSE193677)[60]. The processed public spatial transcriptomics dataset was downloaded from the GEO (accession number GSE189184).

Declarations

Ethics approval and consent to participate

Written informed consent was obtained from the patients, and the study was approved by the Ethics Committee of the First Hospital of Jilin University (22K045-001).

Competing interests

The authors declare that they have no conflicts of interest. We declare that we do not have any commercial or associative interest that presents a conflict of interest in connection with the work.

Received: 21 October 2024 Accepted: 30 April 2025
Published online: 21 May 2025

References

1. Feuerstein JD, Moss AC, Farraye FA. Ulcerative Colitis. Mayo Clin Proc. 2019;94(7):1357–73.
2. Le Berre C, Honap S, Peyrin-Biroulet L. Ulcerative colitis. Lancet. 2023;402(10401):571–84.
3. Olen O, Erichsen R, Sachs MC, Pedersen L, Halfvarson J, Askling J, et al. Colorectal cancer in ulcerative colitis: a Scandinavian population-based cohort study. Lancet. 2020;395(10218):123–31.
4. Jess T, Rungoe C, Peyrin-Biroulet L. Risk of colorectal cancer in patients with ulcerative colitis: a meta-analysis of population-based cohort studies. Clin Gastroenterol Hepatol. 2012;10(6):639–45.
5. Gatenby G, Glyn T, Pearson J, Gearry R, Eglinton T. The long-term incidence of dysplasia and colorectal cancer in a Crohn's colitis population-based cohort. Colorectal Dis. 2021;23(9):2399–406.
6. Ungaro R, Mehandru S, Allen PB, Peyrin-Biroulet L, Colombel JF. Ulcerative colitis. Lancet. 2017;389(10080):1756–70.
7. Little RD, Jayawardana T, Koentgen S, Zhang F, Connor SJ, Boussioutas A, et al. Pathogenesis and precision medicine for predicting response in

inflammatory bowel disease: advances and future directions. eGastroenterology. 2024;2(1).
8. Pisetsky DS. Pathogenesis of autoimmune disease. Nat Rev Nephrol. 2023;19(8):509–24.
9. Guan Q. A comprehensive review and update on the pathogenesis of inflammatory bowel disease. J Immunol Res. 2019;2019:7247238.
10. Abraham C, Cho JH. Inflammatory bowel disease. N Engl J Med. 2009;361(21):2066–78.
11. Parikh K, Antanaviciute A, Fawkner-Corbett D, Jagielowicz M, Aulicino A, Lagerholm C, et al. Colonic epithelial cell diversity in health and inflammatory bowel disease. Nature. 2019;567(7746):49–55.
12. Zhang M, Li X, Zhang Q, Yang J, Liu G. Roles of macrophages on ulcerative colitis and colitis-associated colorectal cancer. Front Immunol. 2023;14:1103617.
13. Liu Y, Zhang L, Ju X, Wang S, Qie J. Single-cell transcriptomic analysis reveals macrophage-tumor crosstalk in hepatocellular carcinoma. Front Immunol. 2022;13:955390.
14. Qi J, Sun H, Zhang Y, Wang Z, Xun Z, Li Z, et al. Single-cell and spatial analysis reveal interaction of FAP+ fibroblasts and SPP1+ macrophages in colorectal cancer. Nat Communicat. 2022;13(1):1742.
15. Bill R, Wirapati P, Messemaker M, Roh W, Zitti B, Duval F, et al. CXCL9:SPP1 macrophage polarity identifies a network of cellular programs that control human cancers. Science. 2023;381(6657):515–24.
16. Davidson S, Coles M, Thomas T, Kollias G, Ludewig B, Turley S, et al. Fibroblasts as immune regulators in infection, inflammation and cancer. Nat Rev Immunol. 2021;21(11):704–17.
17. Aschenbrenner D, Quaranta M, Banerjee S, Ilott N, Jansen J, Steere B, et al. Deconvolution of monocyte responses in inflammatory bowel disease reveals an IL-1 cytokine network that regulates IL-23 in genetic and acquired IL-10 resistance. Gut. 2021;70(6):1023–36.
18. Zhang L, Li Z, Skrzypczynska KM, Fang Q, Zhang W, O'Brien SA, et al. Single-cell analyses inform mechanisms of myeloid-targeted therapies in colon cancer. Cell. 2020;181(2):442-59 e29.
19. Smillie CS, Biton M, Ordovas-Montanes J, Sullivan KM, Burgin G, Graham DB, et al. Intra- and inter-cellular rewiring of the human colon during ulcerative colitis. Cell. 2019;178(3):714-30 e22.
20. Garrido-Trigo A, Corraliza AM, Veny M, Dotti I, Melón-Ardanaz E, Rill A, et al. Macrophage and neutrophil heterogeneity at single-cell spatial resolution in human inflammatory bowel disease. Nat Communicat. 2023;14(1):4506.
21. Mukherjee PK, Nguyen QT, Li J, Zhao S, Christensen SM, West GA, et al. Stricturing crohn's disease single-cell RNA sequencing reveals fibroblast heterogeneity and intercellular interactions. Gastroenterology. 2023;165(5):1180–96.
22. Tang PC, Chung JY, Xue VW, Xiao J, Meng XM, Huang XR, et al. Smad3 promotes cancer-associated fibroblasts generation via macrophage-myofibroblast transition. Adv Sci. 2022;9(1): e2101235.
23. Cheng L, Wang Y, Wu R, Ding T, Xue H, Gao C, et al. New insights from single-cell sequencing data: synovial fibroblasts and synovial macrophages in rheumatoid arthritis. Front Immunol. 2021;12: 709178.
24. Buechler MB, Fu W, Turley SJ. Fibroblast-macrophage reciprocal interactions in health, fibrosis, and cancer. Immunity. 2021;54(5):903–15.
25. Wolf FA, Angerer P, Theis FJ. SCANPY: large-scale single-cell gene expression data analysis. Genome Biol. 2018;19(1):15.
26. Butler A, Hoffman P, Smibert P, Papalexi E, Satija R. Integrating single-cell transcriptomic data across different conditions, technologies, and species. Nat Biotechnol. 2018;36(5):411–20.
27. Hanzelmann S, Castelo R, Guinney J. GSVA: gene set variation analysis for microarray and RNA-seq data. BMC Bioinformatics. 2013;14:7.
28. Jin S, Guerrero-Juarez CF, Zhang L, Chang I, Ramos R, Kuan CH, et al. Inference and analysis of cell-cell communication using cell chat. Nat Commun. 2021;12(1):1088.
29. Efremova M, Vento-Tormo M, Teichmann SA, Vento-Tormo R. Cell PhoneDB: inferring cell-cell communication from combined expression of multi-subunit ligand-receptor complexes. Nat Protoc. 2020;15(4):1484–506.
30. Qiu X, Hill A, Packer J, Lin D, Ma YA, Trapnell C. Single-cell mRNA quantification and differential analysis with Census. Nat Methods. 2017;14(3):309–15.
31. La Manno G, Soldatov R, Zeisel A, Braun E, Hochgerner H, Petukhov V, et al. RNA velocity of single cells. Nature. 2018;560(7719):494–8.
32. Andreatta M, Carmona SJ. UCell: robust and scalable single-cell gene signature scoring. Comput Struct Biotechnol J. 2021;19:3796–8.
33. Van de Sande B, Flerin C, Davie K, De Waegeneer M, Hulselmans G, Aibar S, et al. A scalable SCENIC workflow for single-cell gene regulatory network analysis. Nat Protoc. 2020;15(7):2247–76.
34. Zhao T, Su Z, Li Y, Zhang X, You Q. Chitinase-3 like-protein-1 function and its role in diseases. Signal Transduct Target Therapy. 2020;5(1):201.
35. Sosna B, Aebisher D, Mysliwiec A, Dynarowicz K, Bartusik-Aebisher D, Oles P, et al. Selected cytokines and metalloproteinases in inflammatory bowel disease. Int J Mol Sci. 2023;25(1):202.
36. Bae S, Park PSU, Lee Y, Mun SH, Giannopoulou E, Fujii T, et al. MYC-mediated early glycolysis negatively regulates proinflammatory responses by controlling IRF4 in inflammatory macrophages. Cell Rep. 2021;35(11):109264.
37. Im JH, Buzzelli JN, Jones K, Franchini F, Gordon-Weeks A, Markelc B, et al. FGF2 alters macrophage polarization, tumour immunity and growth and can be targeted during radiotherapy. Nat Communicat. 2020;11(1):4064.
38. Boland BS, He Z, Tsai MS, Olvera JG, Omilusik KD, Duong HG, et al. Heterogeneity and clonal relationships of adaptive immune cells in ulcerative colitis revealed by single-cell analyses. Sci Immunol. 2020;5(50):eabb4432.
39. Nakase H, Sato N, Mizuno N, Ikawa Y. The influence of cytokines on the complex pathology of ulcerative colitis. Autoimmun Rev. 2022;21(3): 103017.
40. Kucharzik T, Koletzko S, Kannengiesser K, Dignass A. Ulcerative colitis-diagnostic and therapeutic algorithms. Dtsch Arztebl Int. 2020;117(33–34):564–74.
41. Kumar A, Smith PJ. Horizon scanning: new and future therapies in the management of inflammatory bowel disease. eGastroenterology. 2023;1(2).
42. Wang X, Khalil RA. Matrix Metalloproteinases, Vascular Remodeling, and Vascular Disease. Adv Pharmacol. 2018;81:241–330.
43. Bai X, Bai G, Tang L, Liu L, Li Y, Jiang W. Changes in MMP-2, MMP-9, inflammation, blood coagulation and intestinal mucosal permeability in patients with active ulcerative colitis. Exp Ther Med. 2020;20(1):269–74.
44. Liu L, Zhang R, Deng J, Dai X, Zhu X, Fu Q, et al. Construction of TME and Identification of crosstalk between malignant cells and macrophages by SPP1 in hepatocellular carcinoma. Cancer Immunol Immunother. 2022;71(1):121–36.
45. Morse C, Tabib T, Sembrat J, Buschur KL, Bittar HT, Valenzi E, et al. Proliferating SPP1/MERTK-expressing macrophages in idiopathic pulmonary fibrosis. Eur Respir J. 2019;54(2):1802441.
46. Kinchen J, Chen HH, Parikh K, Antanaviciute A, Jagielowicz M, Fawkner-Corbett D, et al. Structural remodeling of the human colonic mesenchyme in inflammatory bowel disease. Cell. 2018;175(2):372-86 e17.
47. Martin JC, Chang C, Boschetti G, Ungaro R, Giri M, Grout JA, et al. Single-cell analysis of Crohn's disease lesions identifies a pathogenic cellular module associated with resistance to anti-TNF therapy. Cell. 2019;178(6):1493-508 e20.
48. Rehli M, Niller HH, Ammon C, Langmann S, Schwarzfischer L, Andreesen R, et al. Transcriptional regulation of CHI3L1, a marker gene for late stages of macrophage differentiation. J Biol Chem. 2003;278(45):44058–67.
49. Chen CC, Llado V, Eurich K, Tran HT, Mizoguchi E. Carbohydrate-binding motif in chitinase 3-like 1 (CHI3L1/YKL-40) specifically activates Akt signaling pathway in colonic epithelial cells. Clin Immunol. 2011;140(3):268–75.
50. Kawada M, Seno H, Kanda K, Nakanishi Y, Akitake R, Komekado H, et al. Chitinase 3-like 1 promotes macrophage recruitment and angiogenesis in colorectal cancer. Oncogene. 2012;31(26):3111–23.
51. Qin S, Wang Z, Huang C, Huang P, Li D. Serine protease PRSS23 drives gastric cancer by enhancing tumor associated macrophage infiltration via FGF2. Front Immunol. 2022;13: 955841.
52. Liang T, Tao T, Wu K, Liu L, Xu W, Zhou D, et al. Cancer-associated fibroblast-induced remodeling of tumor microenvironment in recurrent bladder cancer. Adv Sci. 2023;10(31): e2303230.
53. Xie W, Cheng J, Hong Z, Cai W, Zhuo H, Hou J, et al. Multi-transcriptomic analysis reveals the heterogeneity and tumor-promoting role of SPP1/CD44-mediated intratumoral crosstalk in gastric cancer. Cancers. 2022;15(1):164.
54. Kijewska M, Kocyk M, Kloss M, Stepniak K, Korwek Z, Polakowska R, et al. The embryonic type of SPP1 transcriptional regulation is re-activated in glioblastoma. Oncotarget. 2017;8(10):16340–55.

55. Park J, Kim SY, Kim HJ, Kim KM, Choi EY, Kang MS. A reciprocal regulatory circuit between CD44 and FGFR2 via c-myc controls gastric cancer cell growth. Oncotarget. 2016;7(19):28670–83.
56. Wang Z, Pan B, Qiu J, Zhang X, Ke X, Shen S, et al. SUMOylated IL-33 in the nucleus stabilizes the transcription factor IRF1 in hepatocellular carcinoma cells to promote immune escape. Sci Signal. 2023;16(776):eabq3362.
57. Ohsugi T, Yamaguchi K, Zhu C, Ikenoue T, Takane K, Shinozaki M, et al. Anti-apoptotic effect by the suppression of IRF1 as a downstream of Wnt/beta-catenin signaling in colorectal cancer cells. Oncogene. 2019;38(32):6051–64.
58. Gros B, Kaplan GG. Ulcerative colitis in adults: a review. JAMA. 2023;330(10):951–65.
59. Parigi TL, Iacucci M, Ghosh S. Blockade of IL-23: what is in the Pipeline? J Crohns Colitis. 2022;16(2):ii64–72.
60. Argmann C, Hou R, Ungaro RC, Irizar H, Al-Taie Z, Huang R, et al. Biopsy and blood-based molecular biomarker of inflammation in IBD. Gut. 2023;72(7):1271–87.

Publisher's Note